A dynamic cell model for the formation of epithelial tissues*

TATSUZO NAGAI†

Physics Department, Kyushu Kyoritsu University, Kitakyushu 807-8585, Japan

and HISAO HONDA

Faculty of Health Science, Hyogo University, Kakogawa, Hyogo 675-0101, Japan

ABSTRACT

A dynamic model is proposed for monolayered epithelial tissue, in which the monolayer is assumed to consist of prismatic cells, so that the system is described as a two-dimensional polygonal pattern. Its dynamic behaviour is determined by equations of motion for vertices in the polygonal pattern and elementary change in the system (change in the connection of vertex pairs). The vertices are driven by the sum of interfacial tension on cell boundaries and the resistance force against the deformation of cells. It is shown by computer simulations that our model possesses the characteristics of epithelial tissue, that is it has a mechanism which makes the edge number and size of a cell uniform and the shape symmetric. This mechanism finally gives rise to a regular polygonal pattern similar to a honeycomb pattern, even though initial patterns have large variations. Local equilibrium dynamics under which the size of each cell is flexibly adapted to its local environment are compared with non-local equilibrium dynamics. The local equilibrium dynamics produce more natural cellular patterns.

§1. INTRODUCTION

Monolayered epithelial tissue consisting of columnar cells of one cell thickness shows a polygonal cellular pattern on its surface. By observations of developmental and repair processes of the epithelium, the epithelium has been considered to have the ability to make the numbers of edges (or vertices) and the sizes (area) of a polygon homogeneous.

Morphogenesis of chick corneal endothelia (which belong to the epithelial tissue) was observed at several stages during egg incubation and at a few stages after hatching, and the following results were obtained (Kodama *et al.* 1981).

(1) A randomized polygonal cell pattern containing irregular triangular and rectangular cells was produced around day 10 after incubation. The pattern

---

of the edge numbers and sizes of the polygons then began to become homogeneous and showed many five- or six-edge polygons of homogeneous sizes around the stage of hatching (day 21). The cellular pattern of an adult bird showed a pattern consisting of almost regular hexagons.

(2) An extended network of thick bundles of actin filaments (microfilaments) was observed along polygonal cell boundaries as the corneal endothelia developed, using the method of immunofluorescent microscopy with anti-actin antibody. The bundles are considered to have the function of shortening cell boundaries based on an *in-vitro* experiment of cell ghosts where microfilaments are contracted in the medium containing adenosine triphosphate and Mg ions (Owaribe *et al*. 1981).

The healing process of wounded cat corneal endothelia has been documented over intervals as long as 100 days (Honda *et al*. 1982). The corneal endothelium was wounded by removing a small number (about 180) of endothelial cells, and the healing process, that is the movement of cells around the wound, was observed. The surrounding polygonal cells elongated towards the wound, shifted to cover the wound surface and underwent area enlargement. During days 4–7, polygonal cells recovered their non-elongated original regular polygonal shape, but they retained their enlarged size in comparison with that of cells far from the wound.

The shapes of human corneal endothelia were observed after cataract surgery (Kandori *et al*. 1981). Polygonal endothelial cells began to deform from regular polygons after the surgery. The degree of deformation reached an apex 4 weeks later and then decreased. However, recovery towards the original regular polygon was not complete even 12 weeks after the surgery.

On the basis of the above-mentioned observations, the epithelium is considered to have the ability to make polygonal cells with a similar edge number and size to each other, and to make characteristic polygonal patterns. In addition, the observation that the enlarged cell size around the wound in the cat corneal endothelium was retained shows that the local environment around a cell determines the cell size and the environmental effect continues for a long time.

The contractility of cell boundaries in several monolayered cell sheets was estimated using the boundary-shortening procedure (Honda and Eguchi 1980). It was found that the degree of contractility depends on tissue type and is small in tissues belonging to the epithelium. This finding is consistent with the above-mentioned observations of the corneal endothelia. Furthermore, a computer simulation using the boundary-shortening procedure accompanying a topological change (change in the connection of vertex pairs; see figure 2 and § 2 for details) explained the cell rearrangements during the wound healing in a cat corneal endothelium (Honda *et al*. 1982).

Cell rearrangement phenomena were later investigated more generally from the viewpoint that the driving force of the tissue formation is the contractility of cell boundaries. Computer simulations using the extended Potts model (Glazier and Graner 1993) and the equations of motion for Dirichlet cells (Graner and Sawada 1993) were performed in two dimensions. Their results support the viewpoint that contraction of cell boundaries decreases the energy of cell boundaries as a whole and plays an important role in the morphogenesis of epithelial tissues. The purpose of the present paper is to construct a deterministic and dynamic cell model which describes the formation of epithelial tissues from the same viewpoint.

§2. VERTEX DYNAMICS MODEL

In this section we consider a model which describes the formation of epithelial tissues. As mentioned in the preceding section, the model needs to contain a mechanism that makes the edge numbers and sizes of a cell uniform. We therefore add a new mechanism to the vertex dynamics model which modelled the evolution of soap froths and grain aggregates (Nagai *et al.* 1988).

We consider a monolayered sheet consisting of N_c cells where each cell is prism shaped. Assigning the height and base area of cell α to h_α and S_α respectively, we can describe the system by a two-dimensional polygonal pattern and a set $\{h_\alpha\}$ of cell heights. Three straight cell boundaries are assumed to intersect at a vertex of a polygon in the pattern. Then the pattern is described as a system consisting of $2N_c$ vertices connected to one another by straight cell boundaries. Therefore, we can describe the pattern by using a set of variables $\{\mathbf{r}_i, j, j', j''\}$ where $\mathbf{r}_i$ and (j, j', j'') are the position vector and three neighbour vertices respectively of vertex i (figure 1).

2.1. *Tension of the cell boundary*

We consider a mechanism that makes the edge numbers of the cells uniform, which is analogous to surface tension in soap froths and grain aggregates. It is this force that decreases the total energy of cell boundaries; it is given by

$$U_I = \sum_{\langle ij \rangle} \sigma_{\alpha\beta} |\mathbf{r}_i - \mathbf{r}_j|, \tag{1}$$

where $\sigma_{\alpha\beta}$ denotes the boundary energy per unit length between cells α and β, and vertices i and j are at the ends of the boundary line. The sum is taken over all the boundaries $\langle ij \rangle$. The boundary energy per unit length can depend on the type (or the state) of cells α and β. Here we assume that the boundary energy does not depend on the surface area of cell boundary, but on the boundary length. This is because the actin filaments which are considered to give rise to the tension are localized near the apical level of each prism (Owaribe *et al.* 1981).
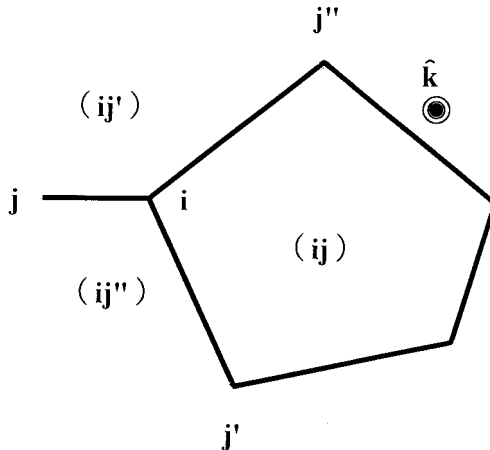

Figure 1. Nearest-neighbour vertices (j, j', j'') of vertex i and notation for cells.

2.2. *Resistance force against cell deformation*

We consider a mechanism that makes the sizes of the cells uniform, which is analogous to the elastic force of elastic bodies. As mentioned in §1, a change in cell area is observed when a cellular pattern varies in monolayered epithelial tissue. This means a change in the base area of the prism in our model. We introduce a force that decreases the total energy of cell deformation; it is given by

$$U_D = \sum_\alpha \rho_\alpha (h_\alpha^0)^2 (S_\alpha - S_\alpha^0)^2, \tag{2}$$

where ρ_α denotes an inherent positive constant of cell α, and h_α^0 and S_α^0 are the equilibrium values of the height and the area respectively of cell α. Here we assume that the cell height is constant. Later we shall discuss the opposite case where the cell height is variable (§7).

2.3. *Equations of motion and elementary process of topological change*

In the vertex dynamics model, the velocity of vertex i is given by

$$\eta \frac{d\mathbf{r}_i}{dt} = -\nabla_i (U_I + U_D), \tag{3}$$

where η is the coefficient of friction. Equation (3) expresses the balance between the frictional force on the left-hand side and the potential force on the right-hand side. The differences in equation (3) from that for the original model of soap froth are that the deformation energy U_D is new and that the coefficient η of friction is assumed to be constant since the number of cells is conserved in the present case (Kawasaki *et al.* 1989). As will be mentioned later (see equation (7)), equation (3) guarantees that each vertex moves so as to decrease the total energy $U = U_I + U_D$.

We derive an explicit form of equation (3) by substituting equations (1) and (2) into it. We designate cells as (ij), (ij') and (ij''), as shown in figure 1, where the three vertices (j, j', j'') are labelled around vertex i in an anticlockwise order. To calculate the right-hand side of equation (3) we use the following two expressions:

$$\nabla_i |\mathbf{r}_i - \mathbf{r}_j| = \frac{\mathbf{r}_i - \mathbf{r}_j}{|\mathbf{r}_i - \mathbf{r}_j|} \tag{4}$$

and

$$\nabla_i S_{ij} = \nabla_i \tfrac{1}{2} \mathbf{k} \cdot [(\mathbf{r}_i - \mathbf{r}_{j''}) \times (\mathbf{r}_{j'} - \mathbf{r}_{j''})] = \tfrac{1}{2}[(\mathbf{r}_{j'} - \mathbf{r}_{j''}) \times \mathbf{k}]. \tag{5}$$

The unit vector $\mathbf{k}$ in equation (5) is perpendicular to the surface of the paper. This vector $\mathbf{k}$ points in the direction in which a right-handed screw moves when it is rotated anticlockwise ($i \to j' \to \cdots \to j''$) inside a cell (ij) (see figure 1). We assume that spatial variation in an equilibrium value S_{ij}^0 is so small that $\nabla_i S_{ij}^0$ is negligible. Then equation (3) becomes

$$\eta \frac{d\mathbf{r}_i}{dt} = -\sum_j^{(i)} \sigma_{ij',ij''} \frac{\mathbf{r}_i - \mathbf{r}_j}{|\mathbf{r}_i - \mathbf{r}_j|} - \sum_j^{(i)} \rho_{ij}(h_{ij}^0)^2 (S_{ij} - S_{ij}^0)[(\mathbf{r}_{j'} - \mathbf{r}_{j''}) \times \mathbf{k}], \tag{6}$$

where the two sums are taken over the three nearest neighbours j of the vertex i.

We describe the topological change in the system by the switching process shown in figure 2. That is, when two vertices connected by an edge come close within an infinitesimal length Δ, they change the connection with their neighbours as shown in
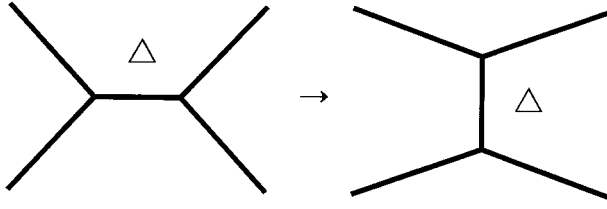
Figure 2. Switching process of neighbour vertices which describes a topological change in the system.

figure 2. In this process the short edge is rotated clockwise by 90° around the middle point of the edge, keeping its length Δ. The length Δ is the shortest length in our model.

Our model consists of the equations of motion given by equation (6) and the switching process shown in figure 2. The equations of motion guarantee that the total energy $U = U_I + U_D$ always decreases whenever each vertex moves according to equation (6), since we have the following general inequality from equation (3):

$$\frac{dU}{dt} = \sum_i \frac{d\mathbf{r}_i}{dt} \cdot \nabla_i U = -\eta \sum_i \left(\frac{d\mathbf{r}_i}{dt}\right)^2 \leqslant 0. \tag{7}$$

On the other hand, the switching process gives rise to a new configuration by changing the connection of vertex pairs and leads to a further reduction in U.

Equation (6) contains five parameters $\eta, \sigma_{\alpha\beta}, \rho_\alpha, h_\alpha^0$ and S_α^0 which, with the exception of η, generally depend on the species of each cell. In this paper, we consider a system which consists of one species and equivalent cells. Hence we shall now drop the subscripts α and β except that we shall consider the α dependence of S_α^0 in and after §5.

The lowest-energy state is the honeycomb pattern which consists of regular hexagons with equal areas in a system consisting of one species of cells. This is because the total length of the cell boundaries is the shortest and there is no deformation in the honeycomb pattern.

When N_c cells exist in a rectangular region of size $L_x \times L_y$, each cell has an area $S^0 = L_x L_y / N_c = (3^{3/2}/2)(l^0)^2$, where l^0 denotes the length of one edge of a regular hexagon and the periodic boundary condition is imposed. Therefore, the lowest total energy of the system is $U = U^0 = 3N_c \sigma l^0$. Generally the total energy is higher than U^0 and also dependent on the coefficient ρ of cell deformation.

§3. ANALYSIS OF THE AVERAGE MOTION OF A CELL

In this section, we shall apply equation (3) to the special case of the symmetric configuration shown in figure 3. Then we shall elucidate the essential properties of the two forces in our model analytically. Furthermore, we shall discuss the condition required as a model for epithelial tissues.

We consider the motion in figure 3 of the central cell which is a regular polygon (edge number n) surrounded by n equivalent hexagons. Four external vertices of each neighbour cell are fixed to make half a regular hexagon with the edge length l^0. Then n vertices of the central cell move radially; for example the point P moves along the
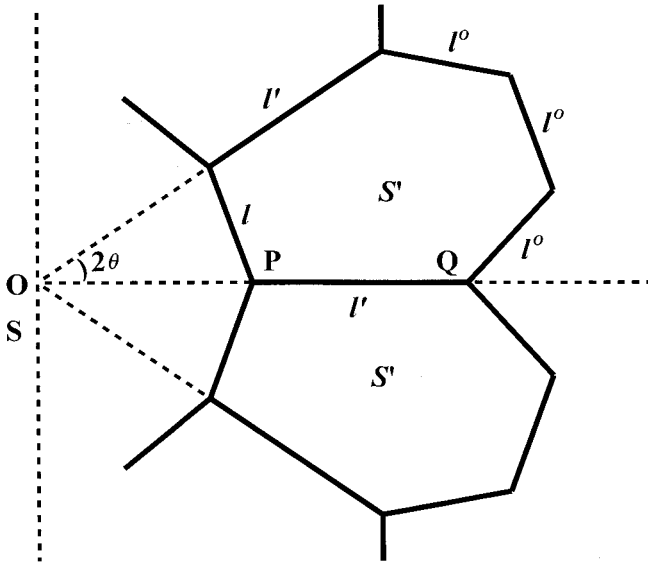
Figure 3. Illustration to explain the analysis of average motion of a cell. There is a symmetric configuration around a regular polygonal cell of edge number n. The central cell is surrounded by n equivalent hexagonal cells. Four external vertices of each hexagonal cell are fixed and compose half a regular hexagon with the edge length l^0 while its two internal vertices are movable: $\theta = \pi/n$.

segment OQ in figure 3. We can choose l (edge length of the central regular polygon) as a unique independent variable since l and l' have the relation given by

$$l' = \frac{(2l^0 - l)}{2\sin\theta} \quad \text{for} \quad 0 < l < 2l^0, \tag{8}$$

where $\theta = \pi/n$ and l^0 denotes the length of one edge of a regular hexagon in the lowest-energy state mentioned in the preceding section.

The cell boundary energy (1) of this subsystem is written as

$$u_{\mathrm{I}} = n\sigma(l + l' + 3l^0)$$
$$= n\sigma\left[\left(1 - \frac{1}{2\sin\theta}\right)l + \left(3 + \frac{1}{\sin\theta}\right)l^0\right]. \tag{9}$$

This expression means that u_{I} is an increasing function of l for $n < 6$, a constant for $n = 6$ and a decreasing function of l for $n > 6$.

On the other hand, the deformation energy (2) of the subsystem is written as follows: defining the area of the central cell by S and those of the n neighbours by S',

$$u_{\mathrm{D}} = \rho(h^0)^2[(S - S^0)^2 + n(S' - S^0)^2]$$
$$= \frac{\rho(h^0)^2}{(4\tan\theta)^2}\{[nl^2 - 6(3)^{1/2}\tan\theta(l^0)^2]^2$$
$$+ n[l^2 - (4 - 3^{3/2}\tan\theta)(l^0)^2]^2\}. \tag{10}$$

Here we have used $S^0 = (3^{3/2}/2)(l^0)^2$ which is the average cell area expressed in the form of a regular hexagon. Equation (10) shows that u_D has one minimum at $l = l_{min}$ for $0 < l < 2l^0$, where l_{min} is given by

$$l_{min} = l^0 \left(\frac{4 + 3^{3/2} \tan \theta}{n+1} \right)^{1/2}. \tag{11}$$

The behaviour of the total energy of the subsystem $u = u_I + u_D$ is determined by competition between u_I and u_D. Equations (9) and (10) show that u is a polynomial of degree 4 with respect to l. Of the four coefficients of the polynomial, the coefficient of the term of degree 1 (see equation (9)) varies only its sign depending on n through θ. It is positive for $n < 6$, zero for $n = 6$ and negative for $n > 6$. Therefore, u has one maximum and one minimum for $n < 6$ while u has one minimum for $n \geqslant 6$. An example of numerical calculation is shown in figure 4.

Figure 4 shows that a cell for $n < 6$ shrinks, vanishing at $l < l_{max}$, where l_{max} denotes the value of l at which u becomes a maximum (arrow in figure 4). In order to prevent the cell from vanishing, we set the following condition:
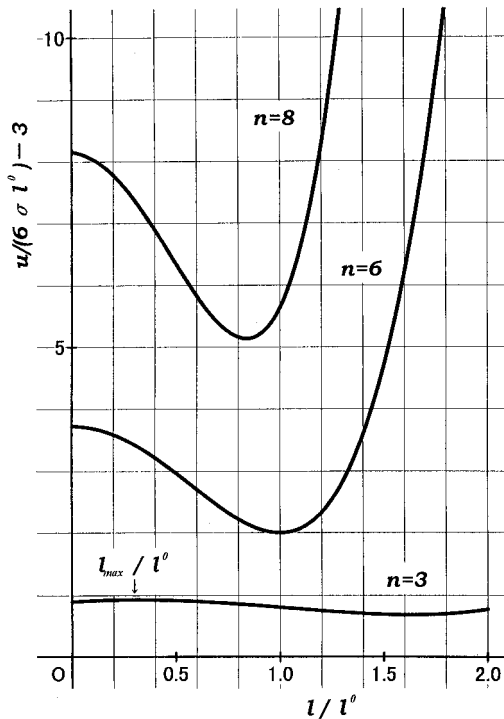
$$l_{max} < \varDelta \ll l^0. \tag{12}$$

Figure 4. Total energy of the subsystem shown in figure 3 in the case of the unique dimensionless parameter $\rho(h^0)^2 (S^0)^{3/2}/\sigma = 5.5$ (see §4). The unit of the vertical axis is $6 \sigma l^0$, which is the cell boundary energy of a regular hexagonal cell. The arrow shows the position of the peak when $l = l_{max}$

Since Δ is the shortest length in our model, l_{max} does not appear. Then the condition that no cell vanishes occurs for equation (12). This inequality limits the range of parameters in our model. When inequality (12) is valid for $n = 3$, it is also valid for $n \geqslant 4$. Hence the sufficient condition that no cell vanishes is given by the condition for $n = 3$:

$$\rho(h^0)^2 S^0 \Delta > \tfrac{18}{13}(3^{1/2} - 1)\sigma. \tag{13}$$

This equation has a simple clear meaning, that is the energy of a cell with linear size Δ is of the order of $\sigma\Delta + \rho(h^0)^2(\Delta^2 - S^0)^2$. The energy becomes $\rho(h^0 S^0)^2$ as the size becomes infinitesimal. The condition that no cell vanishes then requires that the change in energy is positive, that is $2\rho(h^0)^2 S^0 \Delta^2 - \sigma\Delta > 0$, which corresponds to inequality (13) except for numerical factors of the order of one.

§4. Computer simulations

We carried out computer simulations of the vertex dynamics model. Our main interests are to examine whether the model can reproduce the pattern observed in epithelial tissues and to check how much the reproduction depends on the initial state.

First of all, we choose the units of length as the average linear size $\bar{R} = \bar{S}^{1/2}$ of a cell and the unit of time as $\eta\bar{R}/\sigma$, where $\bar{S}$ denotes the average cell area. Then, we have the dimensionless equations of motion for vertices which are obtained by setting $\eta = 1$ and $\sigma = 1$ and regarding other parameters in equation (6) as new dimensionless quantities. Furthermore, we write the new $\rho(h^0)^2$ as ρ again. The newest ρ equals $\rho(h^0)^2\bar{R}^3/\sigma$ in the original units, which is the strength of the resistance force against the cell deformations measured by the tension strength of the cell boundary. Hence there remain three parameters ρ, S^0 and Δ in the newest definitions of variables.

The condition that no cell vanishes (inequality (13)) becomes $\rho\Delta > 1$ in the newest variables, which is reduced to $\rho > 5.0$ since we choose $\Delta = 0.2$ in the following simulation. It should be noted that this is an approximate condition that no cell vanishes, because the condition is obtained for a symmetric configuration of cells.

In this section, we set $S^0_\alpha = 1$ (average cell area) and hence we have only one unknown parameter ρ. We use the random Voronoi cell pattern as the initial state. Based on randomly scattered N_c (number of cells) points, Voronoi cells (or Dirichlet cells) are made around N_c random points. Our system is a rectangle of size $6(N_c/30)^{1/2} \times 5(N_c/30)^{1/2}$ and the periodic boundary condition is imposed on the system. Next we solve the equations of motion by using the Runge–Kutta–Gill method (FACOM Fortran SSL II: RKG) and trace each vertex. Then we calculate the length of each edge at every time step with step size $\delta t = 0.01$. If any edge is shorter than Δ, then it undergoes the switching process shown in figure 2.

Figure 5 shows the result of a simulation for $N_c = 200$ and $\rho = 5.5$. The edge number and size of each cell in the initial Voronoi cell pattern ($t = 0$) demonstrate large variations, as shown in figure 5 (a). As time passes, this variation becomes small and most cells become homogeneous in size, symmetric in shape and six sided, as shown in figure 5 (b) ($t = 0.3$). The pattern varies little after $t = 50$ and hence the pattern ($t = 200$) shown in figure 5 (c) can be regarded as the final state.

We examine typical changes in the size and shape of cells by identifying three cells A, B and C in figures 5 (a)–(c). Cell A is the smallest and four sided at $t = 0$. It is
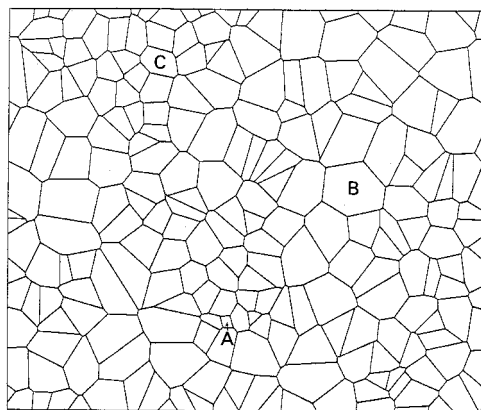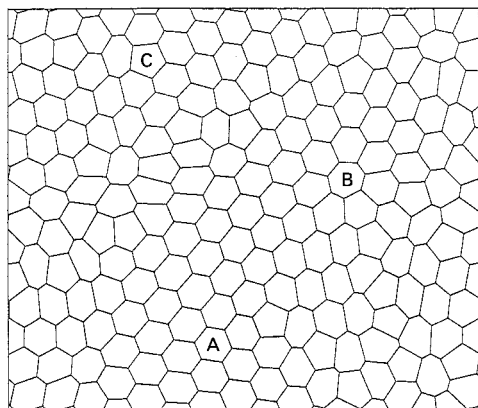
(*a*)
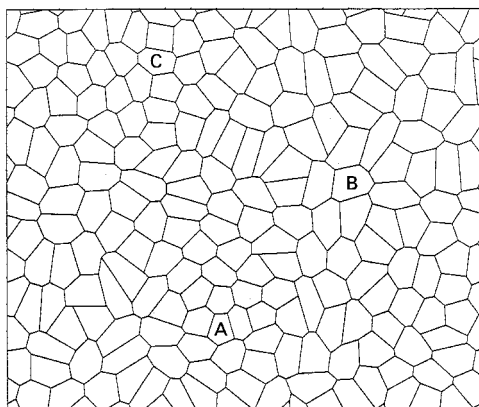
(*b*)

(*c*)

Figure 5.   Snapshots obtained by the simulation with non-local equilibrium dynamics (see §4
and 5) ($N_c = 200$; $\rho = 5.5$): (*a*) $t = 0$; (*b*) $t = 0.3$; (*c*) $t = 200$. A, B and C are cell
identifications (see text).

not crushed but grows with time and becomes close to a regular hexagon of the average size ($t \approx 10$) and little changed until $t = 200$. On the other hand, cell B is the largest and seven sided at $t = 0$. It does not grow but shrinks with time to have the average size and six edges at $t = 10$. However, it has become seven sided again at $t = 200$, as shown in figure 5(c). Cell C has approximately the average size and eight edges at $t = 0$. Finally it becomes a pentagon while its size remains almost constant. These cell behaviours are quite different from those of bubbles in an ideal soap froth, a foam with negligible liquid fraction where a bubble of edge number less than six shrinks, while a bubble of edge number greater than six grows (Glazier and Weaire 1992).

Finally, all cells have become homogeneous in size and shape in this simulation. The final pattern depends on the value of ρ. When $\rho = 1.0$ in the simulation, five cells vanished before $t = 200$. This result is reasonable because the ρ value does not satisfy the condition that no cell vanishes with $\rho\Delta > 1$ with $\Delta = 0.2$.

These simulations show that our model possesses a mechanism to make the edge numbers and sizes of a cell uniform and the shapes symmetric in an appropriate region of parameter values.

In order to have a more quantitative grasp of the above result, we calculated the distribution functions of the edge number and size of a cell from the simulation data. They are defined by $f(n, t)$ and $g(R, t)$, where n and R are the edge number and the linear size (the square root of the area) respectively of a cell. The results are depicted in figures 6 and 7, which show that both functions sharpen as time passes. The final
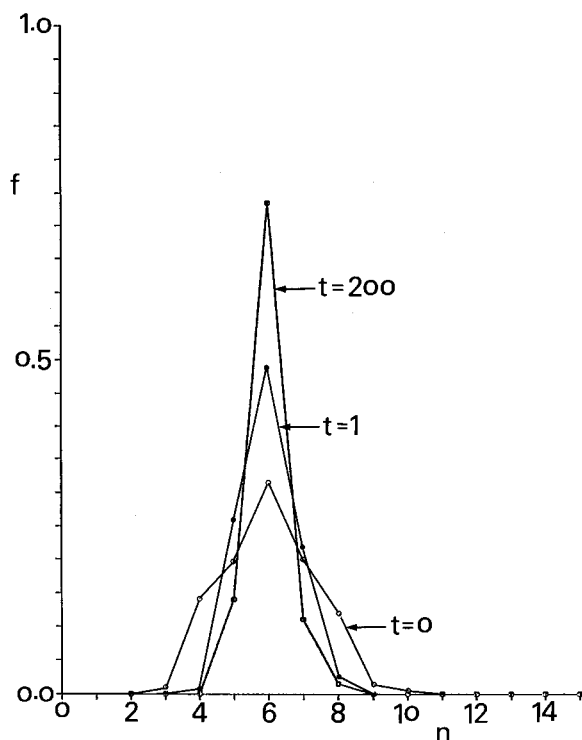

Figure 6. Distribution function $f(n, t)$ of the edge number n of a cell for the patterns in figure 5 at times $t = 0$, 1 and 200.
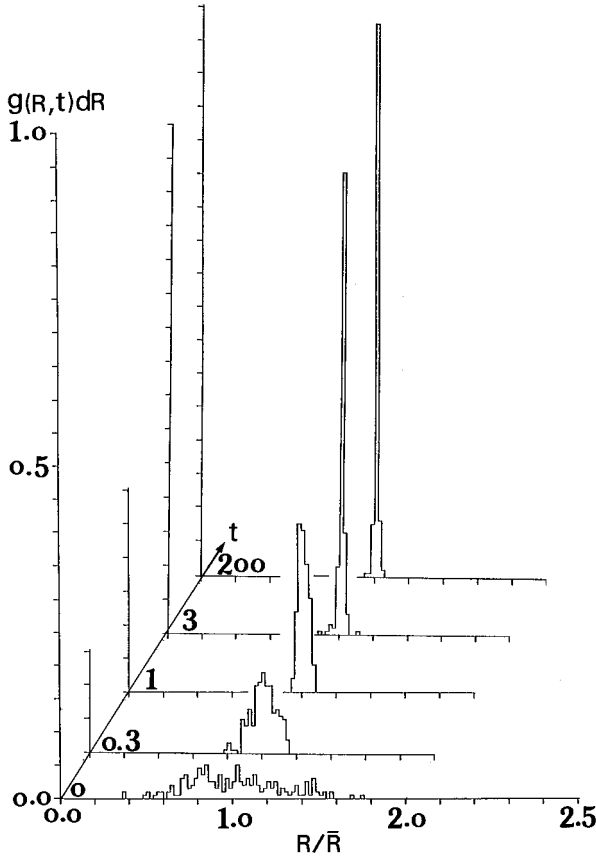
Figure 7. Distribution function $g(R, t)$ of the linear size R of a cell for the patterns in figure 5 at times $t = 0, 0.3, 1, 3$ and 200. The vertical axis shows the probability $g(R, t)\, dR$ that a cell has its linear size between R and $R + dR$, where $dR = 0.02\bar{R}$ ($\bar{R}$ is the average cell size).

distributions of the edge number of a cell are 14, 74, 11 and 1% for $n = 5, 6, 7$ and 8 respectively, and the final distributions of the size of a cell are 8, 83 and 8% for $R/\bar{R} = 0.97$- 0.99, 0.99–1.01 and 1.01–1.03 respectively. Furthermore, to evaluate the sharpness of the distributions we calculated their dispersions defined by

$$\mu_{2f} = \sum_{n=3}^{\infty} (n - \bar{n})^2 f(n, t), \tag{14}$$

$$\mu_{2g} = \int_0^{\infty} dR \left(\frac{R}{\bar{R}} - 1\right)^2 g(R, t), \tag{15}$$

where $\bar{n} = 6$ denotes the average number of edges of a cell and μ_{2g} is dimensionless since $R/\bar{R}$ is chosen as a variable. The results for μ_{2f} and μ_{2g} in the simulation of figure 5 are given at the top of table 1. They both rapidly decrease from $t = 0$ to $t = 10$ and then vary little. The decreasing rate of the size dispersion μ_{2g} is larger than that of the edge number dispersion μ_{2f}.

Table 1.   Time dependence of the dispersion μ_{2f} of edge number distribution and the dispersion μ_{2g} of size distribution for $\rho = 5.5$.

Simulation	S^0		$t = 0.0$	$t = 0.3$	$t = 3.0$	$t = 10.0$	$t = 50.0$	$t = 200.0$
Figure 5	Non-local	μ_{2f}	1.740	0.820	0.430	0.340	0.310	0.310
	($S^0 = 1$)	μ_{2g}	0.721	0.055	0.004	0.001	0.001	0.001
Figure 8	Local	μ_{2f}	1.740	0.840	0.390	0.380	0.380	0.380
	(Constant h)	μ_{2g}	0.721	0.250	0.089	0.061	0.085	0.101
Variable cell	Local	μ_{2f}	1.740	0.730	0.440	0.380	0.380	0.380
height	(Constant V)	μ_{2g}	0.721	0.184	0.064	0.049	0.053	0.056

§5. LOCAL EQUILIBRIUM DYNAMICS

The equilibrium value of cell area has been assumed to be constant throughout the system in the preceding section. However, observations of epithelial tissues showed that the local environment around a cell determines the cell size, as mentioned in §1. In order to incorporate this fact we assume that the equilibrium value S_α^0 of the area of cell α, is determined by

$$S_\alpha^0 = \frac{1}{n_\alpha + 1} \left(S_\alpha + \sum_{\beta=1}^{n_\alpha} S_\beta \right), \tag{16}$$

where n_α denotes the edge number of cell α and the β sum is taken over the immediate neighbour cells of cell α. The right-hand side of equation (16) is the average area of cell α and its neighbour cells at each time. Therefore the equilibrium value S_α^0 is locally determined at each time.

Equation (16) shows that S_α^0 depends on the coordinates of vertices which constitute the cell α and its neighbour cells at each time. Hence, strictly speaking, we need to take the spatial variation in S_α^0 given by equation (16) into account when we derive an explicit form of equation (3) corresponding to equation (6). However, we assume that its spatial variation is so small that $\nabla_i S_{ij}^0$ is negligible, as already mentioned in §2. Then equation (6) also holds in this case. We shall call the time evolution with equation (16) 'local equilibrium dynamics' and the time evolution with S_α^0 uniform throughout the whole system 'non-local equilibrium dynamics' hereafter.

To see the process of equilibration we performed the simulation using local equilibrium dynamics under all the same conditions as used in §4 (figure 5) except for S_α^0. Results are shown in figure 8 and exhibit similar behaviour to those under non-local equilibrium dynamics (figure 5). As time passes, the edge number and sizes of each cell become uniform and its shape becomes symmetric. However, the cell sizes vary from region to region even in the final pattern ($t = 200$ in figure 8 (b)), which are traces of the local heterogeneity of cell size in the initial state ($t = 0$ in figure 5 (a)). The cell size in the final pattern has become more heterogeneous in figure 8 (b) than in figure 5 (c) although the two simulations started with the same initial state.

The three cells labelled A, B and C in figure 8 are the same cells as those in figure 5 at $t = 0$. The three cells in figure 8 change in a similar manner to those in figure 5.
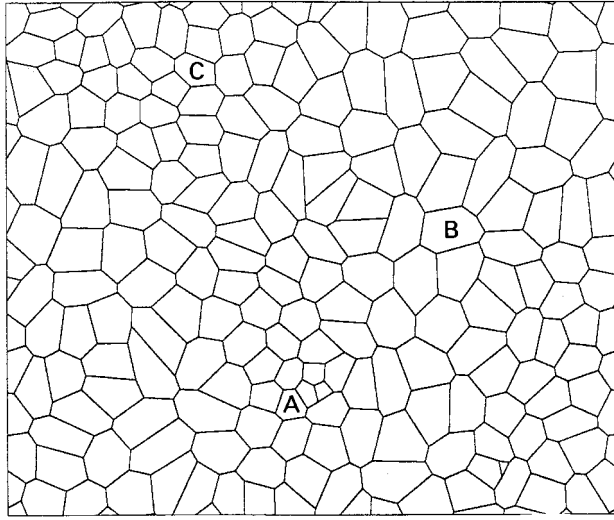
(*a*)
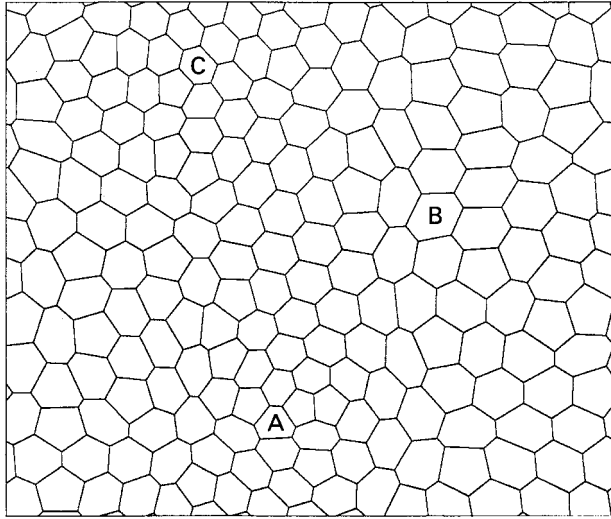
(*b*)

Figure 8. Snapshots obtained by the simulation with local equilibrium dynamics ($N_c = 200$; $\rho = 5.5$): (*a*) $t = 0.3$; (*b*) $t = 200$. The initial pattern ($t = 0$) is the same as the initial pattern ($t = 0$) shown in figure 5 (*a*). A, B and C are cell identifications (see text).

However, we can find the following differences between their final patterns. Cells A, B and C are all six sided in figure 8 (*b*), while they are six, seven and five sided respectively in figure 5 (*c*). They are unequal in size and irregular polygons in figure 8 (*b*), while they are approximately equal in size and regular polygons in figure 5 (*c*). Their sizes still keep their initial local heterogeneity in the final state in figure 8 (*b*), although those have become more heterogeneous.

The dispersions of edge number and cell size in figure 8 were calculated and are given in the middle of table 1. In comparison with those at the top of table 1 (non-

local equilibrium dynamics), the dispersion of edge number changes in almost the same manner, while the dispersion of cell size decreases more slowly with time. The dispersion of cell size becomes larger in local equilibrium dynamics than in non-local equilibrium dynamics in the final state. As shown in figure 8 (a), the size of cells is homogeneous within small regions of dozens of cells, but it shows larger variation over the whole pattern.

The degree of the homogeneity of edge number and cell size in the final state depends on the ρ value, as shown in the following. We examined the ρ dependence of the dispersions in the final state ($t = 200$) by performing simulations with the same initial state under the same conditions except for the ρ value. The result is given in table 2, where δN_c denotes the number of cells which vanished before $t = 200$. The vanishing process was performed in the simulations as follows. When the shortest edge of a triangular cell is less than $\varDelta$, the triangular cell is replaced by a vertex. As shown in table 2, several cells vanished for $\rho \leqslant 5.0$ but no cell vanished for $\rho \geqslant 5.5$. The threshold value corresponds to the condition that no cell vanishes, $\rho > 5.0$ in this case, given by equation (13). Table 2 shows that the dispersion of cell size decreases monotonically as ρ increases while it is difficult to derive a definite tendency of the dispersion of edge number owing to large statistical fluctuation.

Figure 9 shows the effect on the final pattern of varying ρ, taken from the same data as in the case when $\rho = 8.0$ in table 2. Comparing it with figure 8 (b) ($\rho = 5.5$), we see that the cell size in figure 9 has become more homogeneous in the whole region. In fact, table 2 shows that the dispersion of cell size in the case when $\rho = 8.0$ is one third of that in the case when $\rho = 5.5$. The cell size thus becomes more homogeneous through the whole pattern as ρ increases. The ρ value is considered to depend on the system of interest.

In the observation of human corneal endothelia (Kandori *et al.* 1981) mentioned in §1, the distribution of edge numbers of a cell was obtained for 20 normal subjects, ten of a young age group (10–30 years old) and the others of an old age group (60–79 years old). Using their data we calculated the dispersions and obtained $\mu_{2f} = 0.390$ for the young group and $\mu_{2f} = 0.509$ for the old group. Our model explains the difference in μ_{2f} values by the difference in ρ values. We can expect from table 2 that μ_{2f} of the young group is in the range $\rho = 5.5$–9.0 while μ_{2f} of the old group is in

Table 2. ρ dependence of the dispersion μ_{2f} of edge number and the dispersion μ_{2g} of cell size in the final state ($t = 200$). δN_c denotes the number of cells which vanished before $t = 200$. All conditions are the same as those in figure 8 except for the ρ value.

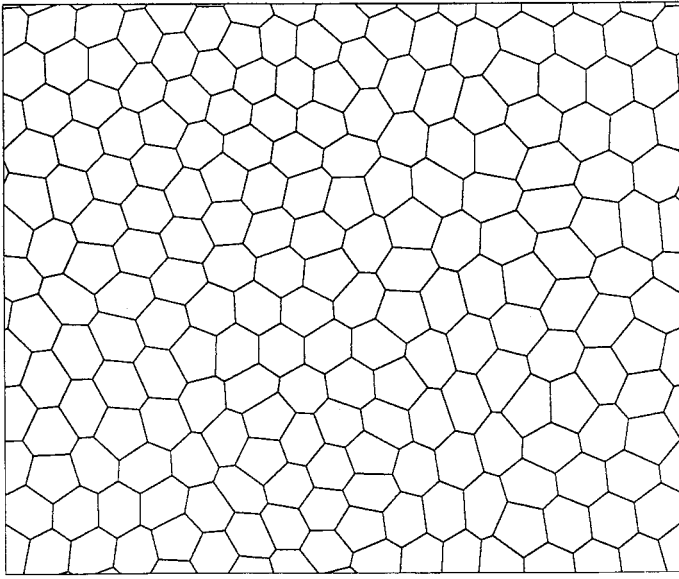| ρ	μ_{2f}	$\mu_{2g} \times 10$	δN_c
1.0	0.400	0.256	35
2.0	0.430	0.366	28
3.0	0.472	0.147	5
4.0	0.361	0.181	6
5.0	0.402	0.187	1
5.5	0.380	0.101	0
6.0	0.320	0.057	0
7.0	0.400	0.039	0
8.0	0.310	0.030	0
9.0	0.390	0.032	0
10.0	0.450	0.018	0

Figure 9. Final pattern ($t = 200$) obtained by the simulation with local equilibrium dynamics ($N_c = 200$; $\rho = 8.0$).

the range $\rho > 10$ since μ_{2f} is considered to become large in the ρ region higher than ten. When we recall that ρ is the strength ratio of resistance force against cell deformation to tension of the cell boundary, it can be considered reasonable that the cells become inflexible or the tensions of cell boundaries diminish on ageing. This is a future problem to examine in detail.

The above-mentioned results show that local equilibrium dynamics give rise to the natural time evolution of the cellular system. Cells which have hereditarily no information about their final states first reach local equilibria by interacting with their neighbour cells and finally complete the total equilibrium of the system after sufficiently long times.

§ 6. INITIAL STATE DEPENDENCE OF THE FINAL STATE

The results obtained up to the preceding section show that, if we choose appropriate values of parameters, our model possesses a mechanism which makes the edge numbers and sizes of a cell uniform and the shapes symmetric without the cell vanishing. Does the mechanism work well in other initial conditions than the random Voronoi cell pattern which was used in the preceding sections? Does it depend on the initial state? We observe common patterns in many real epithelial tissues, where the edge numbers and sizes of a cell are uniform and the shapes are symmetric, in spite of the variety of species. This fact suggests that the final state does not strongly depend on the initial states. To check it in our model, two extreme initial states were examined: firstly, a non-uniform honeycomb pattern which has the shortest total length of cell boundaries (state with the lowest energy of cell boundaries) and, secondly, a uniform square pattern where all cells have the same size (state with the lowest energy of cell deformation).

6.1. *Non-uniform honeycomb pattern*

The initial pattern is shown in figure 10 (*a*) (*t* = 0), where each internal angle of a cell is 120° and cell areas have large variation. The resultant force of three tensions acting on a vertex (the first term on the right-hand side of equation (6)) becomes zero and the resistance force against cell deformation (the second term on the right-hand side of equation (6)) acts upon the vertex in the initial state. The final pattern obtained by the simulation with local equilibrium dynamics is shown in figure 10 (*b*) (*t* = 200). When the resistance force against cell deformation makes the vertex move (to change the cell size to the local equilibrium value) the tensions of cell boundaries always act to keep the 120° structure. The edge number of each cell remains six while the size of each cell rapidly changes into the equilibrium value. In fact, the dispersion of cell size changes as $\mu_{2g} = 0.0451$ (*t* = 0), 0.00002 (*t* = 0.1) and then 0.0000 (*t* = 200). The final state (*t* = 200) is the ideal equilibrium state where all cells are regular hexagons with equal sizes.

6.2. *Uniform square pattern*

The initial pattern is shown in figure 11 (*a*) (*t* = 0), where two vertices are close to each other at a lattice point and are connected by an edge of infinitesimal length $\Delta/20$. Directions of the infinitesimal edges are at random at lattice points although they are invisible in figure 11 (*a*). This initial state is in the opposite extreme to the non-uniform honeycomb pattern, that is the resultant force of three tensions acting upon a vertex is finite while the resistance force against cell deformation is negligibly small. Figure 11 (*b*) (*t* = 200) shows the final pattern obtained by the simulation with the local equilibrium dynamics. The tension causes frequent changes in the edge number of cells, which make the cell size inhomogeneous at early stages in the simulation. Then the resistance force against cell deformation suppresses such changes to make the cell size uniform. The dispersions vary as $\mu_{2f} = 0.920$ (*t* = 0), 1.440 (*t* = 0.1), 0.500 (*t* = 0.3) and 0.180 (*t* = 200) and $\mu_{2g} = 0.0000$ (*t* = 0), 0.0063 (*t* = 0.1), 0.0012 (*t* = 0.3) and 0.0005 (*t* = 200). The two dispersions both increase at the beginning, reach their apexes at around *t* = 0.1 and then decrease. It should be noted that, in the equilibration process with local equilibrium dynamics, the system
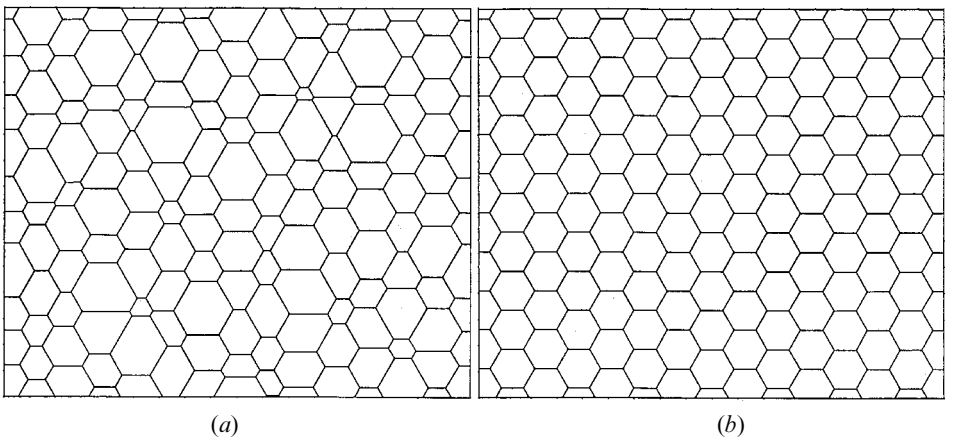

| (*a*) | (*b*) |

Figure 10.   (*b*) Final pattern (*t* = 200) obtained by the simulation with local equilibrium dynamics under (*a*) the initial state of a non-uniform honeycomb pattern (*t* = 0) ($N_c = 140$; $\rho = 8.0$).
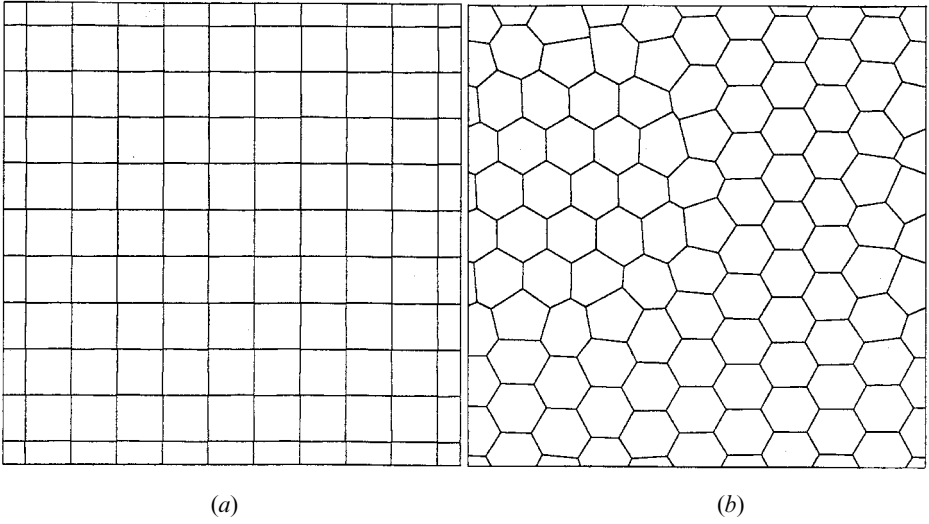
Figure 11. (*b*) Final pattern ($t = 200$) obtained by the simulation with local equilibrium dynamics under (*a*) the initial state of a uniform square pattern ($t = 0$) ($N_c = 100$; $\rho = 8.0$).

makes the edge numbers and sizes of a cell uneven temporarily, and then adjusts them to their optimum values to approach the total equilibrium state. The final state is close to the ideal regular honeycomb pattern as shown in figure 11 (*b*) ($t = 200$).

The two final states of the above-mentioned examples are not identical. Taking the large difference between their initial states into account, we can, however, conclude that the final state depends weakly on the initial state. The interfacial tension and the resistance force against cell deformation cooperatively gave rise to the regular honeycomb-like pattern in our model.

§ 7. Discussion

7.1. *On cell height*

Until the preceding section we have considered the case where the cell height is constant and the cell volume is variable. We here discuss the opposite case where the cell height is variable and the cell volume is constant.

The total energy of cell deformation given by equation (2) can be rewritten as follows (in the original definition of variables):

$$U_D = \sum_\alpha \rho_\alpha (h^0_\alpha S_\alpha - V_\alpha)^2, \tag{17}$$

where $V_\alpha = h_\alpha S_\alpha = h^0_\alpha S^0_\alpha$ is the volume of cell α, which is assumed to be constant. Equation (17) means that the deformation energy of a cell is proportional to the square of the upper cell volume above the level of the equilibrium height. While there is no difference between the two conditions, constant and variable cell heights, in non-local equilibrium dynamics, a difference appears in local equilibrium dynamics, because the equilibrium cell height varies according to $h^0_\alpha = V_\alpha / S^0_\alpha$ with S^0_α given by equation (16) in local equilibrium dynamics.

In order to see the effect of variable cell height, we performed a simulation with local equilibrium dynamics under the same conditions as in § 5 (figure 8) except that

h_α^0 varies in the present case. The dispersions of edge number and size of a cell obtained by the simulation are shown at the bottom of table 1. Comparing them with those of figure 8 (middle of table 1), we see that the μ_{2f} values decrease with time in almost the same manner in both cases while μ_{2g} in the present case of variable cell height decreases more rapidly than in the constant-height case. These results show that the condition of variable cell height and constant cell volume makes the cell sizes more uniform to some extent, in comparison with the condition of constant cell height and variable cell volume, but the difference is not large. Therefore the assumption of constant cell height holds as a first approximation.

7.2. *Comparison between non-local and local equilibrium dynamics.*
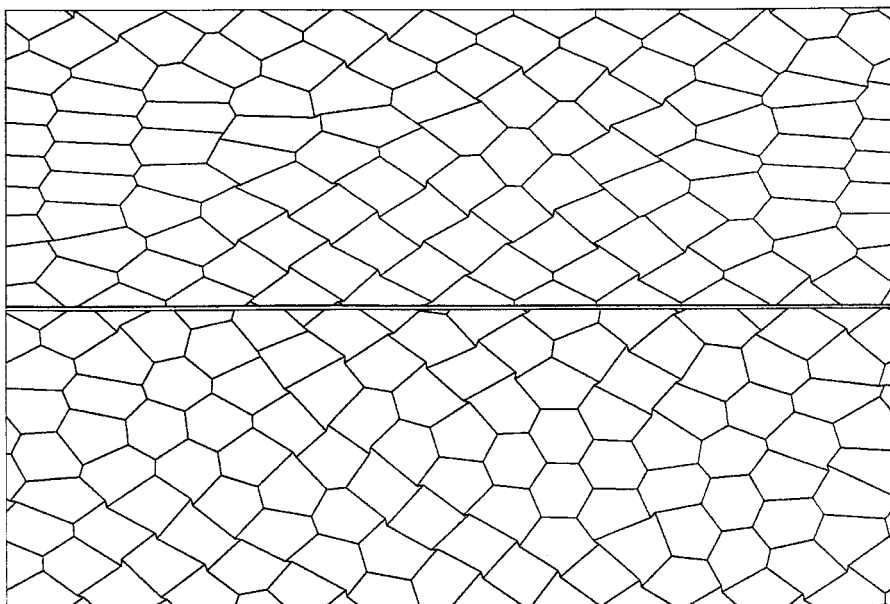
Applying non-local and local equilibrium dynamics to the same initial pattern, we show that the local equilibrium dynamics introduced in §5 enable each cell to adapt more flexibly to its local environment and that it produces a more natural pattern than non-local equilibrium dynamics do.

The initial state ($t = 0$) is shown in figure 12 (*a*). The pattern is modelled on the pattern of elongated cells found in the course of wound healing in the cat corneal endothelium, as mentioned in §1 (Honda *et al.* 1982). Such elongated cells, as seen in figure 12 (*a*), changed into approximately regular polygons a few weeks after the wounding of the cat corneal endothelium. We performed a pair of simulations with the non-local and local equilibrium dynamics using the same initial state as shown in figure 12 (*a*). The cell height was assumed to be constant. Figures 12 (*b*) and (*c*) show the results of non-local equilibrium dynamics and local equilibrium dynamics respectively. In the case of figure 12 (*b*), although several almost regular polygons appear at $t \approx 10$, their number does not increase until $t = 200$ in non-local equilibrium dynamics. On the other hand, in the case in figure 12 (*c*), some almost regular polygons have already appeared at $t = 1$ (upper part of figure 12 (*c*)) and increase in number as time proceeds. In the final state, the cell sizes are kept uniform but the cell shapes do not become regular in non-local equilibrium dynamics (lower part of figure 12 (*b*)), while the cell sizes become uniform and the cell shapes become approximately regular as a whole in local equilibrium dynamics (lower part of figure
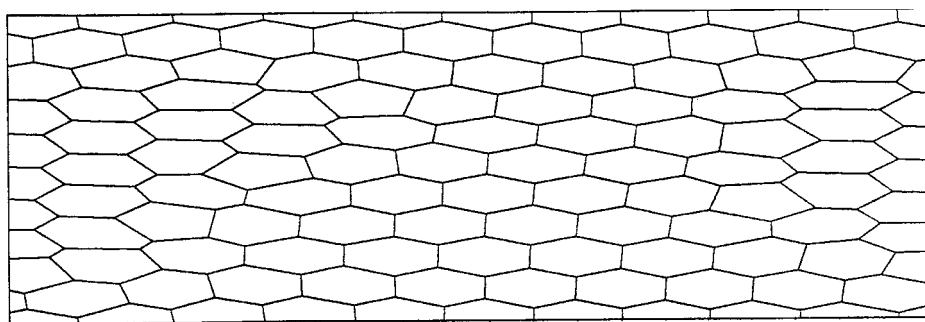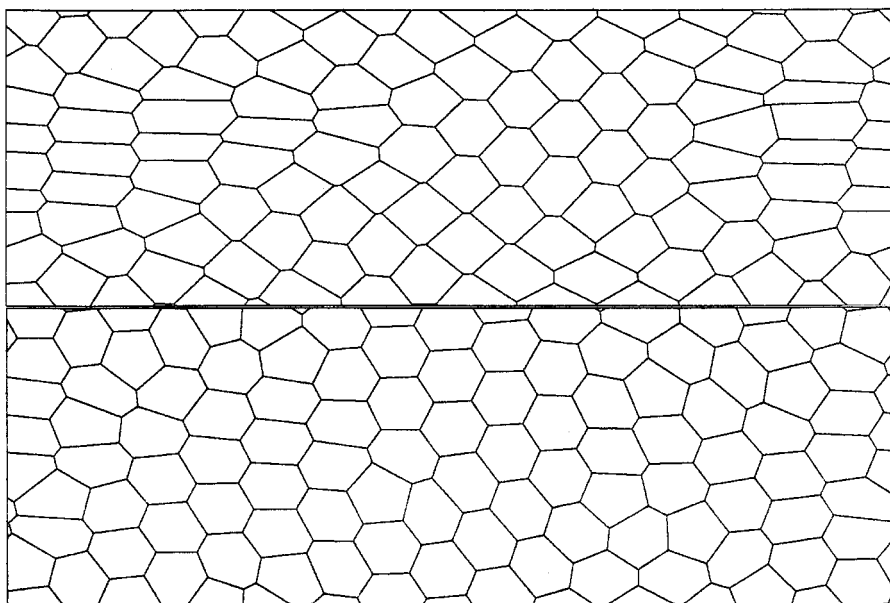

(*a*)

Figure 12.   Snapshots obtained by the simulations with (*b*) non-local and (*c*) local equilibrium dynamics under (*a*) the same initial state ($N_c = 100$; $\rho = 5.5$): (*a*) initial state, $t = 0$; (*b*) with non-local equilibrium dynamics, $t = 1$ (upper), $t = 200$ (lower); (*c*) with local equilibrium dynamics, $t = 1$ (upper), $t = 200$ (lower).

(*b*)

(*c*)

Figure 12.   (*continued*)

12 (*c*)). In fact, while the dispersions of edge number and size of a cell at $t = 0$ are $\mu_{2f} = 0.160$ and $\mu_{2g} = 0.0001$ in both cases, they become, at $t = 200$, $\mu_{2f} = 0.900$ and $\mu_{2g} = 0.0002$ in non-local equilibrium dynamics and $\mu_{2f} = 0.300$ and $\mu_{2g} = 0.0003$ in local equilibrium dynamics.

The pattern formation of realistic epithelial tissues is thus described more naturally by local equilibrium dynamics.

§8. Conclusions

Epithelial tissues have the characteristic properties that the edge numbers and sizes of epithelial cells are generally uniform and their shapes are rather symmetric in comparison with cells in other tissues of animal bodies. In the present paper, these characteristic properties were elucidated to be spontaneously produced by the tension of cell boundaries and the resistance force against cell deformation.

The system which is a monolayer of cells was assumed to be composed of prismatic cells and described in terms of a two-dimensional polygonal pattern. Its time evolution was determined by the equations of motion for vertices and the neighbour switching process. The equation of motion for a vertex was given by the balance equation between the frictional force and the summation of the tension of cell boundaries and the resistance force against cell deformation. We mainly studied the case where the cell height is constant and the cell volume is variable. The opposite case of variable cell height and constant cell volume was also examined. Comparisons between the two simulations showed that their difference can be neglected to a first approximation.

We have obtained, by computer simulation, the following results:

(1) Our model possesses the characteristic mechanism of epithelia that makes the edge numbers and sizes of a cell uniform and the shapes symmetric.
(2) Local equilibrium dynamics, in comparison with non-local equilibrium dynamics, enable each cell to adapt flexibly to its local environment and to produce more natural patterns.
(3) Although we used several patterns (random Voronoi, honeycomb, square and elongated cell patterns) as the initial state, our cell model produces the natural epithelial patterns without a strong dependence on the initial pattern. This explains observations that epithelia show common cellular patterns in spite of the variety of their species.

The above results (1)–(3) suggest that our model gives a basis for describing the observations of morphogenesis of chick corneal endothelia (Kodama *et al*. 1981) and wound healing of cat corneal endothelia (Honda *et al*. 1982) mentioned in §1.

References

GLAZIER, J. A., and GRANER, F., 1993, *Phys. Rev.* E, **47**, 2128.
GLAZIER, J. A., and WEAIRE, D., 1992, *J. Phys.: condens. Matter,* **4**, 1867.
GRANER, F., and SAWADA, Y., 1993, *J. theor. Biol.,* **164**, 477.
HONDA, H., and EGUCHI, G., 1980, *J. theor. Biol.,* **84**, 575.

HONDA, H., OGITA, Y., HIGUCHI, S., and KANI, K., 1982, *J. Morphol.,* **174**, 25.
KANDORI, T., SAWA, M., and TANISHIMA, T., 1981, *Acta Soc. Ophthalmol. Japan,* **85**, 1204 (in Japanese).
KAWASAKI, K., NAGAI, T., and NAKASHIMA, K., 1989, *Phil. Mag.* B, **60**, 399.
KODAMA, R., HONDA, H., and EGUCHI, G., 1981, *Dev. Growth Differences,* **23**, 456 (abstract).
NAGAI, T., KAWASAKI, K., and NAKAMURA, K., 1988, *J. Phys. Soc. Japan,* **57**, 2221.
OWARIBE, K., KODAMA, R., and EGUCHI, G., 1981, *J. Cell Biol.,* **90**, 507.